



Article

Silica Coated Bi₂Se₃ Topological Insulator Nanoparticles: An Alternative Route to Retain Their Optical Properties and Make Them Biocompatible

Blaž Belec ^{1,*}, Nina Kostevšek ², Giulia Della Pelle ^{2,3}, Sebastjan Nemeč ^{4,5}, Slavko Kralj ^{4,5}, Martina Bergant Marušič ⁶, Sandra Gardonio ¹, Mattia Fanetti ¹ and Matjaž Valant ¹

¹ Materials Research Laboratory, University of Nova Gorica, 5000 Nova Gorica, Slovenia

² Department for Nanostructured Materials, Jožef Stefan Institute, 1000 Ljubljana, Slovenia

³ Jožef Stefan International Postgraduate School, 1000 Ljubljana, Slovenia

⁴ Department for Material Synthesis, Jožef Stefan Institute, 1000 Ljubljana, Slovenia

⁵ Faculty of Pharmacy, University of Ljubljana, 1000 Ljubljana, Slovenia

⁶ Laboratory for Environmental and Life Sciences, University of Nova Gorica, 5000 Nova Gorica, Slovenia

* Correspondence: blaz.belec@ung.si

Abstract: Localized surface plasmon resonance (LSPR) is the cause of the photo-thermal effect observed in topological insulator (TI) bismuth selenide (Bi₂Se₃) nanoparticles. These plasmonic properties, which are thought to be caused by its particular topological surface state (TSS), make the material interesting for application in the field of medical diagnosis and therapy. However, to be applied, the nanoparticles have to be coated with a protective surface layer, which prevents agglomeration and dissolution in the physiological medium. In this work, we investigated the possibility of using silica as a biocompatible coating for Bi₂Se₃ nanoparticles, instead of the commonly used ethylene-glycol, which, as is presented in this work, is not biocompatible and alters/masks the optical properties of TI. We successfully prepared Bi₂Se₃ nanoparticles coated with different silica layer thicknesses. Such nanoparticles, except those with a thick, ≈200 nm silica layer, retained their optical properties. Compared to ethylene-glycol coated nanoparticles, these silica coated nanoparticles displayed an improved photo-thermal conversion, which increased with the increasing thickness of the silica layer. To reach the desired temperatures, a 10–100 times lower concentration of photo-thermal nanoparticles was needed. In vitro experiments on erythrocytes and HeLa cells showed that, unlike ethylene glycol coated nanoparticles, silica coated nanoparticles are biocompatible.

Keywords: topological insulator; bismuth selenide; photo-thermal material; biocompatibility; nanoparticles



Citation: Belec, B.; Kostevšek, N.; Pelle, G.D.; Nemeč, S.; Kralj, S.; Bergant Marušič, M.; Gardonio, S.; Fanetti, M.; Valant, M. Silica Coated Bi₂Se₃ Topological Insulator Nanoparticles: An Alternative Route to Retain Their Optical Properties and Make Them Biocompatible. *Nanomaterials* **2023**, *13*, 809. <https://doi.org/10.3390/nano13050809>

Academic Editor:

Isabel Pastoriza-Santos

Received: 3 February 2023

Revised: 15 February 2023

Accepted: 19 February 2023

Published: 22 February 2023



Copyright: © 2023 by the authors. Licensee MDPI, Basel, Switzerland. This article is an open access article distributed under the terms and conditions of the Creative Commons Attribution (CC BY) license (<https://creativecommons.org/licenses/by/4.0/>).

1. Introduction

In the last two decades, topological insulator nanoparticles (TI) have been intensively studied due to their attractive electronic properties, resulting from their metallic, linearly dispersing, and spin-polarized topological surface states (TSS). A TI is like an ordinary insulator in its interior, but it contains protective conductive TSS at the material's borders (surface or edges) [1–4]. The presence of the surface conduction electrons in TSS, which can resonate upon optical excitation, is considered to be the origin of the localized surface plasmon resonance (LSPR) displayed by TI in the low-frequency part of the visible range (>400 nm) [5–7]. Moreover, due to this LSPR, nanoparticles display a photo-thermal effect (PE), which makes them relevant in the field of medical diagnosis and therapy [6,8–14].

A typical representative and one of the most promising TIs, due to a narrow bulk band gap of 0.3 eV, is bismuth selenide (Bi₂Se₃) [15–17]. To fully exploit the exotic properties of Bi₂Se₃ nanoparticles, it is crucial to prepare them without an adsorbent on their surface, which could mask or quench their surface and the optical properties originating from TSS [7].

Despite the interesting properties that make TI nanoparticles relevant for numerous applications, adsorbent-free TI nanoparticles are not suitable for biomedical applications. Nanoparticles without any protective surface layer will agglomerate immediately when they are subjected to a physiological medium (e.g., serum, cell culture, blood). In addition, the protective surface layer also counteracts the possible dissolution of the nanoparticles and prevents the leakage of potentially toxic metal ions. The surface layer can be used for further functionalization [18–22].

There is a scarcity of reports regarding the application of Bi_2Se_3 nanoparticles in biomedicine and their effects *in vivo* and *in vitro* [6,8–14]. A major challenge is to prevent their oxidation and instability, which limits their practical applications [13]. To date, this problem has been solved by preparing Bi_2Se_3 nanoplatelets through the solvothermal method, using ethylene-glycol (EG) and polyvinylpyrrolidone (PVP) as the solvent and capping agent, respectively. Reports claimed that stability and biocompatibility were achieved using PVP molecules attached to the surface of Bi_2Se_3 nanoparticles [9,12,13,23–28]. However, in 2018, we showed that the solvothermal method, where EG and PVP were used, resulted in Bi_2Se_3 nanoplatelets only coated with an approximately 2 nm thick EG layer. This was confirmed by ζ -potential measurements and TG-MS analyses. These analyses did not show the presence of PVP [7].

Since it was shown that Bi_2Se_3 nanoparticles produced via the solvothermal method are coated with EG, which is toxic, this raises safety concerns for using such Bi_2Se_3 nanoparticles in biomedical applications. Despite the beneficial properties of EG, such as reducing the surface charges and therefore improving the colloidal stability in the physiological environment, prolonging the nanoparticles' half-life and preventing potential dissolution, EG can affect the central nervous, cardiopulmonary, and renal systems, and its metabolites can cause numerous deleterious effects at the cellular level, e.g., oxidative stress [29–32]. In addition, the Food and Drug Administration (FDA) only approved EG for use indirectly, as a component of packaging adhesives in the food industry [33]. Moreover, further functionalization of EG-coated Bi_2Se_3 nanoparticles is challenging, because it often requires chemicals that are expensive, toxic, or unstable, and the synthetic procedures require personnel with the appropriate laboratory skills (e.g., human serum albumin, doxorubicin—a drug for treating cancer, etc.) [10,11].

Based on the described drawbacks of using EG as a coating, there is a need to prepare Bi_2Se_3 nanoplatelets coated with a non-toxic, stable, and biocompatible layer that allows further easy functionalization and does not mask the optical properties of Bi_2Se_3 , as EG does. The most similar molecule, and less toxic than EG, is polyethylene glycol (PEG), which can be used as a coating and is already the gold standard for biocompatible coatings. PEGylation of nanoparticles is commonly used in liposomes and other nanoparticles to increase the circulation time and slow the rate of elimination by the reticuloendothelial system. However, despite the widespread use of PEG in food and drugs, people have started to show an immune response by developing anti-PEG antibodies, which can lead to the rapid elimination of PEG-coated nanoparticles [34–37].

Therefore, one solution to replace EG or PEG could be porous amorphous silicon dioxide (silica). Unlike EG, silica is approved by the Food and Drug Administration (FDA) and European Food Safety Authority (EFSA) as non-toxic and biodegradable, with an uptake of up to 1500 mg/day [38–40]. Moreover, it has an excellent porous structure, adjustable pore size, and easily modified surface [38,41–44]. Due to these properties, silica nanoparticles have great potential for biomedical applications (i.e., cancer therapy, DNA transfection, drug delivery, dental medicine, regenerative medicine, etc.) [45–48]. As a coating material, silica is used in combination with various functional nanomaterials [49,50], i.e., magnetic nanoparticles [51–59], luminescent nanoparticles [48,60,61], and photo-thermal responsive nanomaterials [49,56,62] etc., making them biocompatible and extending their applicability through further functionalization.

In this work, we successfully coated Bi_2Se_3 nanoparticles with layers of silica of different thicknesses. As mentioned earlier, a coating can mask or impair the optical

properties of the TI nanoparticles derived from the TSS. Silica-coated Bi₂Se₃ nanoparticles retain these optical properties, except for those with the thickest, ≈ 200 nm, silica layer. Silica-coated nanoparticles exhibit good photo-thermal properties and specific adsorption rate (SAR) values. In vitro experiments showed that pristine (hydrothermally prepared) and silica-coated Bi₂Se₃ nanoparticles do not induce hemolysis and are not cytotoxic, even at very high concentrations of up to 1 g/L.

2. Materials and Methods

2.1. Materials

All the chemicals were used without further purification.

Bi₂Se₃ nanoparticles synthesis: Bismuth (III) nitrate pentahydrate (Bi(NO₃)₃·5H₂O), bismuth (III) oxide (Bi₂O₃, 99.98%), selenium powder (Se, $\geq 99.5\%$), hydrochloric acid (HCl), hydrazine hydrate (N₂H₄·H₂O, 35%), sodium hydroxide (NaOH), ethylene glycol (C₂H₆O₂, 99%), polyvinylpyrrolidone (PVP, MW = 8000). All chemicals were purchased from Alfa Aesar, Haverhill, MA, USA.

Amorphous silica coating: Hexadecyltrimethylammonium bromide (CTAB) was obtained from Alfa Aesar (Kandel, Germany), absolute ethanol and aqueous ammonia ($\sim 25\%$) from Merck KGaA (Darmstadt, Germany), cyclohexane from VWR Int. GmbH (Vienna, Austria), tetraethoxysilane (TEOS), concentrated hydrobromic acid ($\sim 48\%$; HBr) and 2-amino-2-(hydroxymethyl)-1,3-propanediol (TRIS) from Sigma-Aldrich (St. Louis, MO, USA); 0.1 M HBr was prepared by diluting concentrated HBr ($\sim 48\%$) with deionized water.

Hemolysis: Erythrocytes were isolated from whole sheep blood (BioSap SO, defibrinated, purchased from AdvaMed d.o.o., Ljubljana, Slovenia). Phosphate-Buffered Saline tablets (PBS) (Sigma Aldrich, St. Louis, MO, USA), potassium chloride (KCl), and sodium chloride (NaCl).

In vitro cell viability assay: Dulbecco's modified Eagle's medium (DMEM) (Gibco, Paisley, UK), fetal bovine serum (FBS) (Gibco, Paisley, UK), Penicillin Streptomycin (Gibco, Grand Island, NY, USA), 2.5% Trypsin (10X) (Gibco, Paisley, UK), phosphate-buffered saline (PBS) (Gibco, Paisley, UK), PrestoBlue Viability Reagent (Invitrogen, Eugene, OR, USA).

2.2. Methods

2.2.1. Synthesis of Bi₂Se₃ Nanoparticles

The Bi₂Se₃ nanoparticles were prepared using the hydrothermal method, according to the procedure described in Ref. [7]. In short, stoichiometric amounts of bismuth nitrate (1 mmol) and selenium (1.5 mmol) were dissolved in 20 mL of deionized water under vigorous stirring, followed by the addition of 11 M HCl (25 μ L) and hydrazine (1.6 mL). The obtained grey slurry was sealed in a Teflon-lined autoclave and heated at 240 °C for 48 h. Then the product was washed several times with deionized water. This sample was denoted as "BiSe". Afterwards, the clean, adsorbent-free platelets were coated with amorphous SiO₂ (silica) of different thicknesses. The coating procedures are described below.

To compare and evaluate the effect of silica coating, the Bi₂Se₃ nanoparticles were also prepared by the solvothermal method, according to the procedure described in Ref. [63]. In brief, PVP and stoichiometric amounts of Bi and Se were dissolved in 20 mL of ethylene glycol. The grey slurry was sealed in a Teflon-lined autoclave and heated to 200 °C for 10 h. After the reaction had finished, the product was washed several times with deionized water. The solvothermally-synthesized platelets were denoted as "BiSe ST".

2.2.2. Coating of Bi₂Se₃ Nanoparticles with Amorphous Silica

Thin silica coating: First, a thin silica coating (2–5 nm) was deposited on the platelets. The procedure was based on Ref. [64]. In a glass beaker, 320 mg of CTAB was dissolved in 40 mL of deionized H₂O. Then, the pH of the formed CTAB solution was adjusted to 3.30 using 0.1 M HBr. Separately, 200 mg of dried adsorbent-free BiSe platelets were dispersed

in 18 mL of deionized H₂O using intense mixing with a magnetic stirrer and simultaneous ultrasonication with a sonicator (VibraCell 505; Sonics & Materials Inc., Newtown, CT, USA). The formed BiSe suspension was added to the acidic CTAB solution. The pH of the formed mixture of CTAB and BiSe platelets was adjusted to pH 2.85 with 0.1 M HBr. Then, a solution of 2.8 mL of TEOS in 5.2 mL of absolute ethanol was added, and the reaction mixture was stirred at room temperature for 90 min. After that time, the pH of the reaction mixture was increased to 5.0 using diluted aqueous ammonia, and the reaction mixture was further stirred at room temperature overnight. Then, the silica-coated nanoparticles were collected using centrifugation for 10 min at 7000× *g*, washed several times with ethanol and water, and finally dispersed in 10 mL of water. The sample was denoted as “**BiSe@S-thin**”.

Intermediate silica coating: To obtain an intermediate, 50–80 nm thick silica coating, BiSe@S-thin platelets were used as a starting material. In a flat bottom flask, 10 mL of the BiSe/s-thin aqueous suspension was added and diluted with 40 mL of deionized water. Then, 12 mL of aqueous ammonia (~25%) was added. The mixture was sonicated for 5 min in an ultrasound bath (Sonis 4, Iskra PIO, Šentjernej, Slovenia). After sonication, a solution of 0.7 mL of TEOS in 45 mL of absolute ethanol was added. The formed reaction mixture was further sonicated for 5 min in an ultrasound bath and stirred with a mechanical shaker overnight at ≈200 rpm. Finally, the silica-coated nanoparticles were collected using centrifugation for 10 min at 7000× *g*, washed several times with ethanol and water and dispersed in 10 mL of H₂O. The sample was denoted as “**BiSe@S-interm**”.

Thick silica coating: To obtain a thick, ≈200 nm thick silica coating, BiSe@S-interm platelets were used as a starting material. In a flat bottom flask, 10 mL of the BiSe/s-interm aqueous suspension was diluted with 30 mL of deionized water. Then, 4.8 mL of aqueous ammonia (25%) was added, followed by the addition of a solution of 2.0 mL TEOS in 90 mL absolute ethanol. The formed reaction mixture was sonicated for 5 min in an ultrasound bath and stirred with a mechanical shaker overnight at ≈200 rpm. Finally, the coated nanoparticles were collected using centrifugation for 10 min at 7000× *g*, washed several times with ethanol and water and dispersed in 10 mL of water. The sample was denoted as “**BiSe@S-thick**”.

2.2.3. Synthesis of Silica Spheres

Silica spheres (*d* ≈ 200 nm) were synthesized using the following procedure. First, 50 mL of deionized water, 40 mL of absolute ethanol, and 9 mL of aqueous ammonia (≈25%) were mixed in a glass flat-bottom flask. Then, a solution containing 3 mL of TEOS and 10 mL of absolute ethanol was added to the glass flask containing water, ethanol, and ammonia. The formed reaction mixture was left to stir on a mechanical shaker overnight. The next day, the formed silica spheres were sedimented using centrifugation at 7000× *g* for 10 min and washed several times with ethanol and deionized water. The silica spheres were finally re-dispersed and stored in deionized water.

2.2.4. Analysis Methods

The synthesized product was characterized using an X-ray powder diffractometer Rigaku MiniFlex (Tokyo, Japan) (with Cu K α radiation (λ -1541 Å, 30 kV, 10 mA). For the TEM analysis, the platelets were suspended in ethanol and deposited on a copper-grid-supported lacy carbon film. The TEM analysis was performed using a field-emission electron microscope (JEOL JEM 2100UHR, Tokyo, Japan) operating at 200 kV and equipped with an Oxford X-Max80T energy dispersive X-ray spectroscopy detector (EDXS). The width of the platelets expressed as the equivalent diameter was determined from the TEM images, on which 200–300 platelets per sample were utilized for the statistic using Gatan Digital Micrograph Software (Pleasanton, CA, USA). The obtained data, representing the frequency count of the size distribution, were fitted using single or multiple peak Gaussian fit modes. The electrochemical properties (ζ -potential) of the platelets dispersed in water were measured as a function of the suspension pH using a ZetaPALS instru-

ment (Brookhaven Instruments Corporation, Holtsville, NY, USA). The pH of the aqueous suspension was adjusted with diluted hydrochloric acid and sodium hydroxide.

The light absorption properties were analyzed using classical UV-vis spectroscopy. Spectroscopy was performed with a PerkinElmer Lambda 950 spectrometer (Walham, MA, USA), using a quartz cuvette with a size of $1 \times 1 \times 3$ cm. A measurement range, λ , from 200 to 850 nm was used, with a scanning rate of 1 nm/s. Before the measurements, the water suspension of the platelets was stabilized according to the ζ -potential and sonicated to break any possible agglomerates.

Photo-thermal experiments were performed using an FC-808 Fiber Couple Laser System (CNI Optoelectronics Tech, Changchun, China) configured for continuous-wave operation at 808 nm, with different powers. Laser light was focused on a quartz cuvette with a size of $1 \times 1 \times 3$ cm using an optical lens focusing on a spot size of 8 mm. Control (water) and samples with different concentrations (0.1, 0.3, 0.5, and 1 g/L) were irradiated at a laser power $P = 3 \text{ W/cm}^2$ for 5 min. To test the stability, the samples were cycled 2 times (5 min on, 5 min off). The temperature of the liquid samples was measured with a J-type Teflon thermocouple, which was immersed in the cuvette and connected to a computer to collect the data in real-time. The specific adsorption rate was calculated as follows:

$$\text{SAR} = \frac{\rho C_s}{m_{\text{sample}}} \left(\frac{\Delta T}{\Delta t} \right)_{t=0}$$

where ρ and C_s are the effective density and effective specific heat capacity of the sample, respectively, $m_{\text{Bi}_2\text{Se}_3}$ is the total content of nanoparticles in the sample (g/cm^3), and $\left(\frac{\Delta T}{\Delta t} \right)_{t=0}$ is the slope of the photo-thermal curve linear fit. The $\Delta T/A$ values were calculated by dividing the change of the temperature obtained after 5 min with adsorption measured at 808 nm. In the investigated system, the Bi_2Se_3 nanoparticles represent the photo-thermal material. In the case of the uncoated nanoparticles, $m_{\text{sample}} = m_{\text{Bi}_2\text{Se}_3}$, while in the case of the coated one, $m_{\text{sample}} = m_{\text{Bi}_2\text{Se}_3} + m_{\text{coating}}$. Due to this, the concentration of photo-thermal active particles was calculated for each coated sample by calculating the mass share of Bi_2Se_3 nanoparticles and the surface layer (silica or EG). For the calculation of the Bi_2Se_3 nanoparticle mass, the average particle diameter of 175 nm (size distribution = 50–300 nm), the thickness of 10 nm, and density $\rho = 6.82 \text{ g/cm}^3$ were taken. For the silica layer, the average thicknesses, i.e., 3 nm, 65 nm, and 200 nm, for thin, intermediate, and thick silica layers, respectively, and $\rho = 2 \text{ g/cm}^3$ was taken. In the case of the solvothermally-synthesized nanoparticles, the correction was made similarly, but taking into account a diameter of nanoparticles of 300 nm, thickness of 10 nm, and EG layer thickness of 2 nm. The ρ of the EG was 1.1 g/cm^3 .

2.2.5. Hemotoxicity Test

A phosphate-buffered saline (PBS) buffer was prepared by dissolving PBS tablets (Sigma Aldrich, St. Luis, MO, USA) in Milli-Q autoclaved water, to a final concentration of 0.01 M phosphate buffer, 0.0027 M potassium chloride, and 0.137 M sodium chloride. A hemolysis study was performed on the erythrocytes isolated from whole sheep blood. Briefly, whole blood was centrifuged at 800 rpm for 20 min, and the buffy coat was subsequently removed. Erythrocytes were re-dispersed in PBS 1 \times , 7.4, at 5% *v/v* for further analysis. Then, 1 mL of erythrocytes were incubated in triplicate with different concentrations of each nanoparticle sample for 3 h at 37 °C with constant orbital shaking. After incubation, tubes were centrifuged (1500 rpm/4 min) to sediment cells, and the supernatant was analyzed in triplicates. The hemolysis was evaluated by measuring the absorbance of the released hemoglobin (*A*) at 541 nm in the supernatant using a spectrophotometer (BioTek Synergy H4 Hybrid microplate reader, Winooski, VT, USA). Each sample was measured in triplicate. Samples representing “100% dead” were prepared by lysing control samples with deionized water via hypotonic osmotic shock, while samples representing “0%” as a negative control were simply incubated with buffer. The hemolysis

was then calculated as follows: $Hemolysis (\%) = 100 (A_{sample} - A_{control}) / (A_{100\% \text{ dead}} - A_{control})$. Mixed-effect ANOVA (Graphpad 8.1, Prism) was used to test whether the nanoparticle-correlated hemolysis was significantly higher than the negative control. Data are presented as the mean \pm standard deviation (SD) for all experiments.

2.2.6. In Vitro Cell Viability Assay

HeLa cells (ATCC CCL-2) were grown at 37 °C in a humidified atmosphere and 5% CO₂. The growth medium was DMEM, supplemented with 10% FBS, 100 µg/mL penicillin, and 100 µg/mL streptomycin. The medium was changed every 2–3 days. When the cells reached 70–90% confluence, they were detached with a 0.25% trypsin solution and subculture at a 1:5 ratio. Nanoparticles (2 g/L) in PBS were diluted in the growth medium, to obtain final concentrations of 0.1, 0.3, 0.5, and 1 g/L. The viability of the samples exposed to different concentrations of nanoparticles was compared with pure PBS diluted in the same ratio with growth medium. Untreated (mock-treated) cells served as a negative control for the viability calculations (value 1). HeLa cells were seeded at 2×10^4 cells/well in a 96-well microtiter plate and grown overnight. Cells were then exposed to nanoparticles or PBS in the growth medium. After incubation in a cell incubator for 24 h, the cells were washed with PBS and incubated with 10% PrestoBlue Viability Reagent in a growth medium for 1.5 h. The viability of HeLa cells was determined by measuring the metabolic conversion of the PrestoBlue resazurin-based dye to highly fluorescent resorufin using an Infinite F200 plate reader (Tecan, Grödig, Austria) at 560 nm excitation and 595 nm emission. The fluorescence intensities obtained were corrected for background fluorescence and normalized to mock-treated HeLa cells. Three independent experiments, each with three technical replicates, were performed to evaluate the viability of the HeLa cells. Cells were analyzed using two-way ANOVA. Dunnett's multiple comparisons test was used to compare cells exposed to PBS only with cells exposed to different nanoparticles at the same concentrations. Tukey's multiple comparisons test was used to compare different concentrations within each treatment. Multiplicity-adjusted P values were calculated for each comparison. Statistical analyses of the in vitro toxicity assays were performed using GraphPad Prism 8 software (GraphPad Software, San Diego, CA, USA).

3. Results and Discussion

To investigate the possibility of using silica coating as an alternative to EG coating, the hydrothermally synthesized, adsorbent-free Bi₂Se₃ nanoparticles were coated with silica layers of three different thicknesses. To evaluate the effect of the surface silica layer, the coated nanoparticles were compared with their solvothermally-prepared (EG-coated) counterparts [63].

Figure 1 shows the XRD patterns of the hydrothermally- and solvothermally-synthesized Bi₂Se₃ nanoparticles (BiSe and BiSe-ST, respectively). The diffraction patterns are very similar. The peaks in both cases can be indexed according to the rhombohedral structure of Bi₂Se₃ (space group *R3m*, JCPDS 33-0214). The strong and sharp diffraction peaks indicate that the Bi₂Se₃ nanoparticles were well crystallized. The TEM analysis of BiSe and BiSe-ST nanoparticles showed that the nanoparticles had a hexagonal plate-like morphology. As was expected according to theory [65], the size distribution of the hydrothermally synthesized nanoparticles was broader (majority with $d \approx 50\text{--}300$ nm, a minority with $d > 300$ nm) compared to the size distribution of their BiSe-ST counterparts ($d \approx 280\text{--}380$ nm) [7]. EDXS analysis showed that the platelets had an atomic ratio Bi/Se = 0.66 ± 0.1 , which was in good agreement with Bi₂Se₃ stoichiometry. As was shown in our previous study, the most important difference between the BiSe and BiSe-ST nanoparticles was only observed with HR-TEM, when the nanoparticles were orientated edge-on, with their large surface parallel to the electron beam. While the BiSe nanoparticles were clean, the BiSe-ST nanoparticles were coated with a thin, approximately 2 nm thick, ethylene-glycol layer (see Ref. [7] for more details).

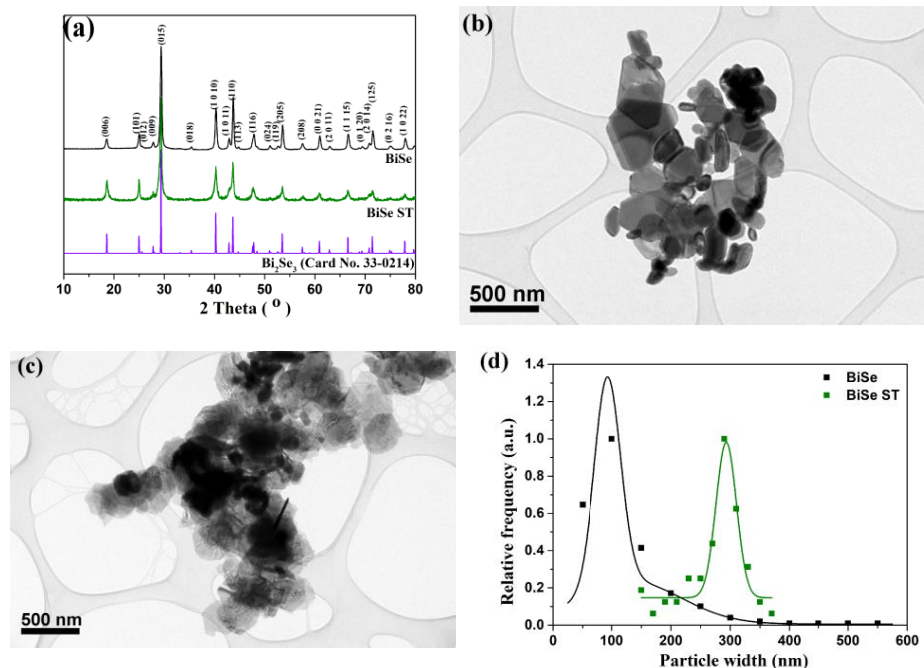


Figure 1. XRD patterns of Bi_2Se_3 nanoparticles synthesized hydrothermally (BiSe) and solvothermally (BiSe ST) (a). Representative TEM image of BiSe (b) and BiSe-ST (c) nanoparticles, and the corresponding size distribution (d), obtained from TEM images.

Figure 2 shows the BiSe nanoparticles subsequently coated with (a) a thin $\approx 2\text{--}5$ nm, (b) an intermediate $\approx 50\text{--}80$ nm, and (c) a thick ≈ 200 nm uniform silica layer covering the individual nanoparticles. An additional confirmation that the silica coating was successful was the change in the point of zero charges (PZC). Figure 2d shows the zeta potential (ζ) of the silica-coated BiSe nanoparticles compared to the uncoated ones and silica nanospheres synthesized using a modified Stober process [64]. The PZC decreased from $\text{pH} = 5$ (BiSe) to ≈ 2.5 for BiSe@S-thin and ≈ 3 for BiSe@S-thick.

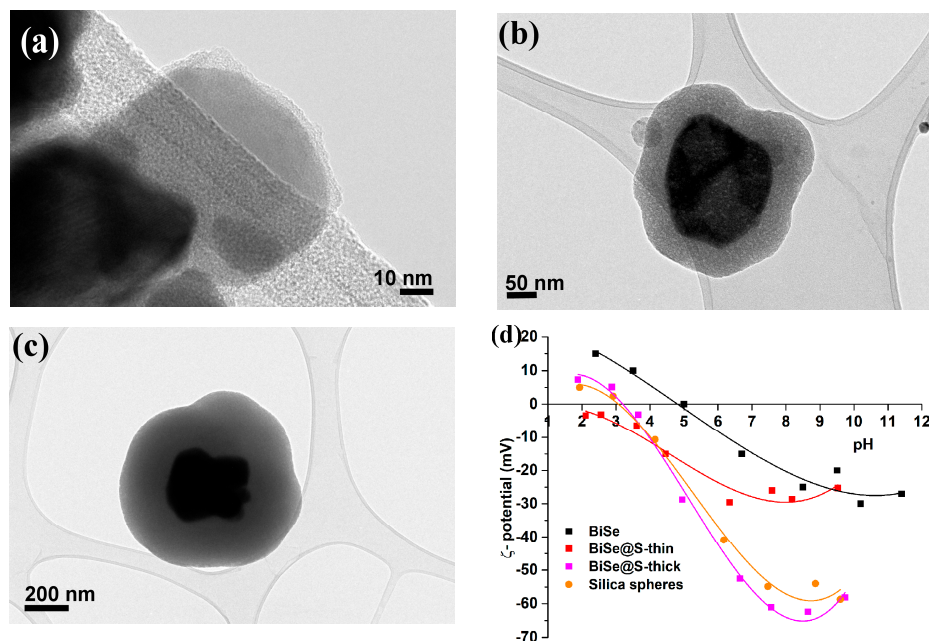


Figure 2. TEM image of silica-coated Bi_2Se_3 nanoparticles with thin $\approx 2\text{--}5$ nm (a), intermediate $\approx 50\text{--}80$ nm (b) and thick ≈ 200 nm silica layer (c). Zeta-potential behavior of silica-coated Bi_2Se_3 nanoparticles compared to uncoated nanoparticles and silica nanospheres (d).

In our previous work [7], we demonstrated that an EG layer, adsorbed on the surface of the Bi_2Se_3 nanoparticles, can mask/impair the optical properties derived from TSS. Namely, BiSe-ST nanoparticles display absorption peaks in the range of $\approx 200\text{--}350$ nm and $\approx 350\text{--}550$ nm. Near the IR region, the absorbance decreases without showing absorption peaks [7]. On the contrary, the absorption spectrum of BiSe nanoparticles in the spectral range of $\approx 200\text{--}300$ nm is very similar to that of BiSe-ST. However, a striking difference can be observed at higher wavelengths, where BiSe nanoparticles display an intense and broad adsorption peak over the entire measured range. This broad peak can be ascribed to LSPR, which results from TSS [5]. Figure 3 shows the normalized UV-Vis absorption spectra of the silica-coated Bi_2Se_3 nanoparticles compared to their BiSe and BiSe-ST counterparts. Normalization of UV-Vis spectra was used to qualitatively evaluate the impact of the coating layer on the optical properties of the Bi_2Se_3 nanoparticles. The BiSe@S-thin and BiSe@S-interm samples displayed similar absorption spectra to the BiSe nanoparticles over the entire measuring area. They showed absorption peaks in the spectral range $\approx 210\text{--}300$ nm, where both BiSe and pure silica spheres adsorb. At a higher wavelength, they showed a broad adsorption peak, dominating over the whole measured spectral region from ≈ 380 to 850 nm, which can be ascribed to the LSPR resulting from TSS. The only difference in the adsorption of BiSe@S-thin and BiSe@S-interm compared to the BiSe sample was a less pronounced absorption peak in this region, which can be attributed to the silica coating. However, the results suggest that the thin ($\approx 2\text{--}5$ nm) and intermediate ($\approx 50\text{--}80$ nm) silica layers did not mask the optical properties derived from TSS. With the increase in the silica layer thickness, the absorption spectrum also changed. In the spectral range from $\approx 200\text{--}350$ nm, the BiSe@S-thick sample displayed absorption spectra very similar to the BiSe, BiSe@S-thin, and BiSe@S-inter samples. Towards higher wavelengths, the absorption of the BiSe@S-thick sample decreased, similarly to the case of the BiSe-ST sample.

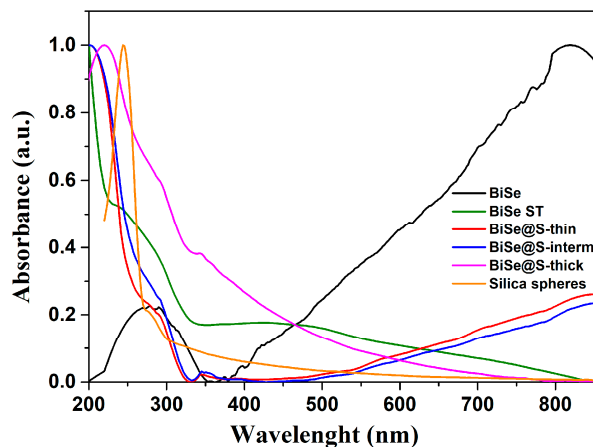


Figure 3. Normalized UV-Vis absorption spectra of the silica-coated nanoparticles with the thin ($\approx 2\text{--}5$ nm), intermediate ($\approx 50\text{--}80$ nm), and thick (≈ 200 nm) silica layer in comparison with the clean, EG coated nanoparticles, and silica spheres. The measurement was done on a suspension with a concentration of 0.1 g/L.

According to theory [66], nanoparticles that display LSPR also display a photo-thermal effect, i.e., the effect in which a material can convert light into heat [67]. This effect makes TI nanoparticles relevant for biomedical applications, which has been reported previously [6,8–14]. Figure 4a shows the photo-thermal performance of the silica-coated Bi_2Se_3 nanoparticles suspended in water at a concentration of 0.1 g of particles/L. The results were compared with the performance of the BiSe and BiSe-ST counterparts. The measurements show that the BiSe@S-thin and BiSe@S-interm samples exhibited better photo-thermal conversion, while the sample BiSe@S-thick exhibited a similar conversion to the BiSe sample. Compared to the solvothermally-prepared nanoparticles (BiSe-ST), the silica-coated nanoparticles showed a much lower photo-thermal conversion. The recovery

after the 1st cycle was $\geq 94\%$ for the uncoated and the silica-coated nanoparticles, while the recovery of the BiSe-ST samples was only $\approx 83\%$ (Figure 4b). The photo-thermal conversion of the nanoparticles increased linearly with increasing suspension concentration (Figure 4c). The final temperature obtained after 5 min for each sample and the concentration was measured in triplicate. The difference was less than $0.5\text{ }^{\circ}\text{C}$, which could be attributed to a systematic error of the thermocouple. The determined specific adsorption rate (SAR) showed that the silica-coated nanoparticles had a significantly higher SAR compared to their BiSe counterparts ($\approx 760\text{ W/g}$). The SAR values of the silica-coated nanoparticles decreased when increasing the thickness of the silica layer ($\approx 1150\text{ W/g}$, $\approx 1080\text{ W/g}$, $\approx 940\text{ W/g}$ for BiSe@S-thin, BiSe@S-interm and BiSe@S-thick, respectively). However, the highest SAR was determined for the BiSe ST sample ($\approx 2400\text{ W/g}$) (Figure 4d). To date, there have been no reports of the SAR of Bi_2Se_3 nanoparticles, which is a very important parameter for the determination of the quality of photo-thermal materials. It describes the ability of a material to adsorb radiation per mass unit. Compared to the previous photo-thermal material, Au-nanorods ($\approx 10\text{ kW/g}$) [67], the coated Bi_2Se_3 nanoparticles displayed a moderate SAR. Another parameter describing the quality of photo-thermal materials is $\Delta T/A$, which describes the efficiency of a material in converting adsorbed light into heat (Figure 4e). BiSe ST, the sample with the highest SAR, displayed the lowest conversion efficiency, which was even lower than BiSe. In contrast, the silica-coated nanoparticles showed higher $\Delta T/A$ values compared to the BiSe and BiSe ST samples.

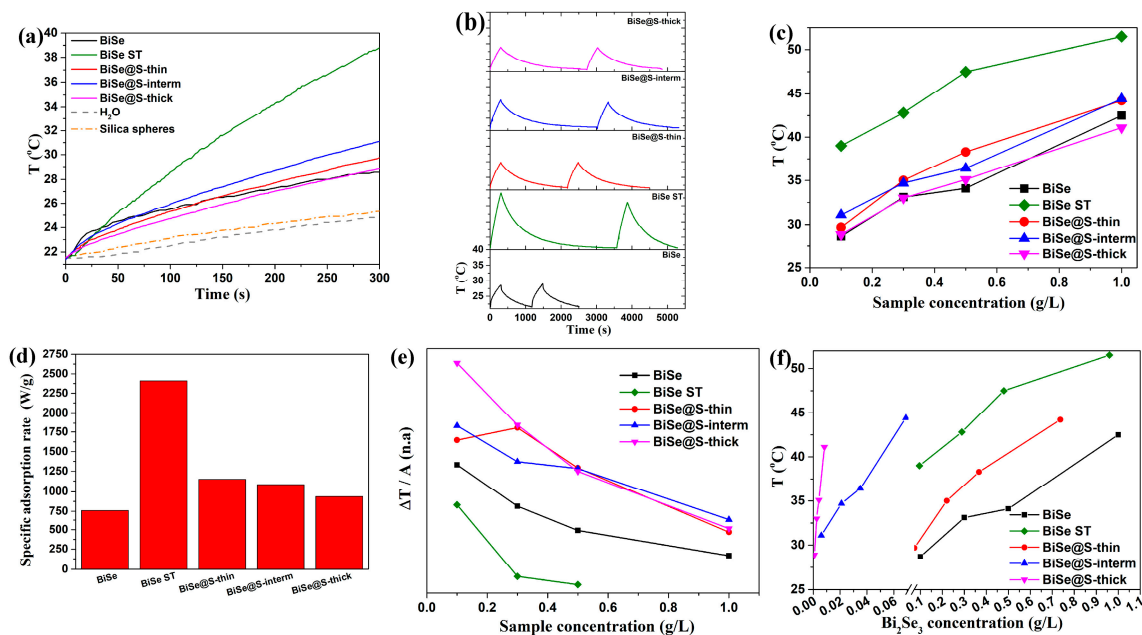


Figure 4. Temperature increase of the particle solution with 0.1 g/L (a) and corresponding heating and cooling cycles (b). Final T reached after 5 min laser exposure at different concentrations (c), specific adsorption rate (SAR) (d) and efficiency of adsorbed light conversion into heat represented as $\Delta T/A$ for different concentrations (e). Final temperatures after 5 min laser exposure vs. concentration of the photo-thermal active particles in the sample (f). The experiments were conducted with laser light of 808 nm and $P = 3\text{ W/cm}^2$.

When determining photo-thermal properties, the concentration/mass of the photo-thermal particles that actually perform the photo-thermal conversion is essential. In our system, the Bi_2Se_3 nanoparticles represent the photo-thermal part of the material that absorbs light and converts it into heat. For the uncoated nanoparticles (BiSe), the mass of the photo-thermal active material was equal to the overall nanoparticle mass. In the case of coated nanoparticles, the mass of the nanomaterials is the sum of the photo-thermal core and the mass of the coating, either EG or silica. Taking this into account,

the photo-thermal conversions shown in Figure 4a,c do not represent the true photo-thermal values of Bi_2Se_3 nanoparticles alone, but of the Bi_2Se_3 and silica coating together. Namely, at a certain concentration, the amount of the photo-thermal active nanoparticles for the BiSe sample was equal to the mass of the sample, while in the case of the coated BiSe-ST, BiSe@S-thin, BiSe@S-interm, and BiSe@S-thick samples, the mass of the photo-thermal active particles was $\approx 3.6\%$, $\approx 26.6\%$, $\approx 93\%$, and $\approx 99.1\%$ lower, respectively, which was due to the coating (more details in the experimental section). To show the actual photo-thermal conversion of the Bi_2Se_3 nanoparticles, the final temperatures obtained after 5 min had to be plotted as the temperature at a certain concentration of Bi_2Se_3 nanoparticles in the sample (Figure 4f). Here, we see that the silica coating enhanced the photo-thermal conversion. The conversion of BiSe@S-thin was slightly improved compared to BiSe but was lower compared to BiSe-ST. When increasing the silica layer, the photo-thermal conversion increased. The BiSe@Si-interm and BiSe@Si-thick samples displayed significantly higher conversion compared to the BiSe, BiSe-ST, and BiSe@S-thin samples. The desired temperatures could be achieved with a lower concentration of photo-thermal active nanoparticles. For instance, a temperature in the range of 43–45 °C (temperature needed for the cell apoptosis [68–71]) was reached with significantly lower concentrations of photo-thermal active nanoparticles than in the case of the BiSe, BiSe-ST, and BiSe@S-thin samples.

This increase in the photo-thermal conversion of the silica-coated nanoparticles compared to the uncoated nanoparticles is consistent with reports in the literature. Namely, the silica shell was transparent to visible and near-IR radiation. In addition to its protective role, the silica coating also improved the thermodynamic stability of the nanoparticles in suspension, and by suppressing light reflection, it improved the light absorption of nanoparticles [72,73]. The same can also be concluded for the EG-coated nanoparticles. The high photo-thermal conversion ($>94\%$) obtained over multiple cycles and sufficient SAR values make silica-coated nanoparticles good candidates for photo-thermal mediators in biomedical applications.

Nanoparticles for biomedical applications must be non-toxic. Figure 5a shows the hemotoxicity of the samples. The mixed-effect ANOVA test, which compared samples with the PBS (negative control), showed that the hemolysis effect was significantly higher for BiSe@S-interm at 0.3 and 0.5 g/L. However, at a concentration of 1 mg/mL for the same sample, the hemolysis was found to be 0.3%. Therefore, this discrepancy falls within the range of experimental method error, and we can conclude that the sample did not cause significant hemolysis. In all cases, the determined hemolysis was lower than 2%, which falls within the error area of the method and indicates that neither the BiSe and BiSe-ST nor silica coated Bi_2Se_3 nanoparticles were hemotoxic under the given conditions.

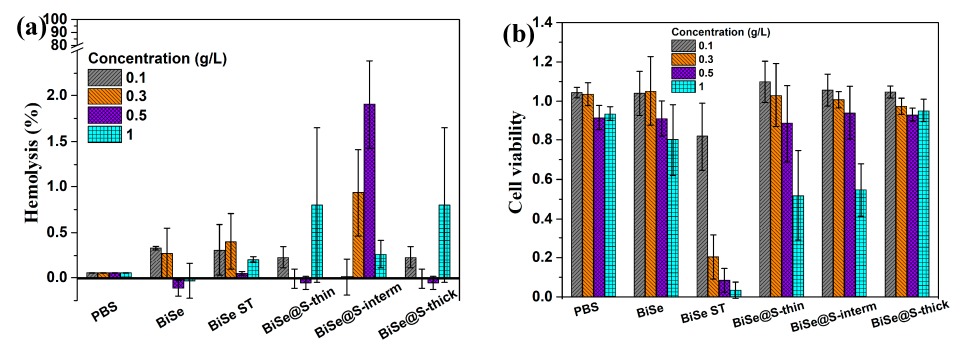


Figure 5. Influence of silica coated Bi_2Se_3 nanoparticles compared to their pristine and ethylene glycol coated counterparts on red blood cells toxicity (a) and HeLa cell viability (b). Cells were exposed to different concentrations of nanoparticles and compared with the control (PBS medium). Negative control for hemotoxicity was 0%, and control for HeLa cell viability was 1.

The biocompatibility of the silica-coated nanoparticles was further tested on a more complex biological system of human cell lines. Figure 5b shows the viability of the HeLa cells after 24 h of exposure to the nanoparticles, with test concentrations ranging from 0.1 to 1 g/L. No significant decrease in cell viability was observed at the lowest concentration of 0.1 g/L compared with PBS for all tested materials (two-way ANOVA, Dunnett's multiple comparisons test). However, at higher concentrations (0.3–1 g/L), the viability of cells exposed to EG-coated nanoparticles was significantly reduced, whereas no significant decrease in cell viability was observed with the pristine or silica-coated Bi₂Se₃ nanoparticles. The viability of cells exposed to BiSe, BiSe@S-thin, and BiSe@S-interm decreased slightly at concentrations higher than 0.5 g/L, whereas BiSe@S-thick showed a similar cell viability to the control, even at higher concentrations. In contrast, the BiSe ST nanoparticle cell viability decreased to 80% at 0.1 g/L, and this effect was even more pronounced at higher concentrations (20%, 10%, and ≈0% cell viability for 0.3, 0.5, and 1 g/L, respectively).

To date, there have been few reports of the use of EG-coated Bi₂Se₃ nanoparticles as photo-thermal mediators for potential biomedical applications [9–12]. No cytotoxicity was observed at lower concentrations, but with concentrations ≥1 g/L, the viability was significantly reduced [10,11], which was similar to our results. The in vitro assay on HeLa cells confirmed our predictions and is consistent with the reported limitations, whereby EG-coated nanoparticles are toxic and, therefore, not appropriate for biomedical applications. On the other hand, the silica-coated Bi₂Se₃ nanoparticles showed an almost negligible cytotoxic effect and are therefore more suitable for biomedical applications.

4. Conclusions

LSPR is responsible for the occurrence of a photo-thermal effect in Bi₂Se₃ TI nanoparticles, which makes them relevant in the field of medical diagnostics and therapy. However, a problem that limits the application of Bi₂Se₃ in the mentioned field is colloidal instability and oxidation in the physiological medium [13]. Therefore, the nanoparticles have to be coated with a protective surface layer. However, in the case of the TI, a protective layer can alter or mask the surface and optical properties originating from TSS, as was demonstrated in the case of an EG coating [7].

There have been reports where EG coated Bi₂Se₃ nanoparticles were used as photo-thermal mediators in biomedical applications [6,8–14]. However, as shown in this work, EG coated nanoparticles are cytotoxic and, therefore, not suitable for clinical applications.

The alternative is a protective surface layer made of silica, which, unlike EG, is FDA and EFCA-approved, being non-toxic and biodegradable. As we demonstrated here, silica coated Bi₂Se₃ nanoparticles with thin (≈2–5 nm) and intermediate (≈50–80 nm) thick silica layer do not alter or mask the optical properties that originate from TSS, as is observed in the case of their EG coated counterparts. A change in the optical properties only appears in the case of the thickest (≈200 nm) silica layers. Here, a thick silica layer probably masks the true optical properties of the TI.

Compared to the uncoated and EG coated Bi₂Se₃ nanoparticles, the silica coated nanoparticles displayed an improved photo thermal effect, which increased with an increasing silica layer. The desired temperatures could be reached with 10–100 times lower concentrations of photo-thermal active nanoparticles compared to their uncoated and EG coated counterparts. With in vitro tests performed on erythrocytes and HeLa cells, we showed that, unlike EG coated nanoparticles, the silica coated nanoparticles are biocompatible. Silica coated Bi₂Se₃ nanoparticles displayed negligible hemolysis and cytotoxicity, even at high concentrations (>0.5 g/L). Nevertheless, although uncoated Bi₂Se₃ nanoparticles are biocompatible, however, they cannot be used in biomedical applications, since they are not colloidal and chemically stable in the physiological medium.

An improved colloidal stability, easy functionalization, high photo-thermal conversion, moderate SAR, and biocompatibility show that silica is a suitable alternative for coating and, therefore, such silica-coated Bi₂Se₃ nanoparticles are a suitable candidate photo-thermal material for biomedical applications.

Author Contributions: B.B. planned and coordinate the study. B.B. performed the synthesis of Bi₂Se₃ nanoparticles, XRD, microscopy, UV-Vis and photo-thermal measurements. S.N. and. S.K. performed silica coating of the Bi₂Se₃ nanoparticles. S.N. performed ζ-potential measurements. B.B., G.D.P., N.K. performed hemotoxicity tests. M.B.M. performed cell toxicity tests. M.V., contributed to conceiving the methodology and interpreting results. S.G., M.F., contributed in the representation of the results. All the authors contributed their part to writing the manuscript. All authors have read and agreed to the published version of the manuscript.

Funding: The work was financially supported by the Slovenian Research Agency, research core funding No. P2-0412 and P2-0089, postdoctoral project No. Z2-2644, ARRS project No. J23034, J2-3040, J2-3046, J3-3079, J7-4420 and bilateral ARRS project No. BI-FR/23-24-PROTEUS-005.

Institutional Review Board Statement: Not applicable.

Informed Consent Statement: Not applicable.

Data Availability Statement: The data presented in this study are available on request from the corresponding author.

Acknowledgments: We would like to acknowledge Slovenian Research Agency for funding the research.

Conflicts of Interest: The authors declare no competing financial interests.

References

1. Hasan, M.Z.; Kane, C.L. Colloquium: Topological insulators. *Rev. Mod. Phys.* **2010**, *82*, 3045–3067. [[CrossRef](#)]
2. Cha, J.J.; Koski, K.J.; Cui, Y. Topological insulator nanostructures. *Phys. Status Solidi (RRL)* **2013**, *7*, 15–25. [[CrossRef](#)]
3. Qi, X.-L.; Zhang, S.-C. Topological insulators and superconductors. *Rev. Mod. Phys.* **2011**, *83*, 1057–1110. [[CrossRef](#)]
4. Kou, L.; Ma, Y.; Sun, Z.; Heine, T.; Chen, C. Two-Dimensional Topological Insulators: Progress and Prospects. *J. Phys. Chem. Lett.* **2017**, *8*, 1905–1919. [[CrossRef](#)]
5. Yin, J.; Krishnamoorthy, H.N.S.; Adamo, G.; Dubrovkin, A.M.; Chong, Y.; Zheludev, N.I.; Soci, C. Plasmonics of topological insulators at optical frequencies. *NPG Asia Mater.* **2017**, *9*, e425. [[CrossRef](#)]
6. Guozhi, J.; Peng, W.; Yanbang, Z.; Kai, C. Localized surface plasmon enhanced photothermal conversion in Bi₂Se₃ topological insulator nanoflowers. *Sci. Rep.* **2016**, *6*, 25884. [[CrossRef](#)]
7. Belec, B.; Ferfolja, K.; Goršak, T.; Kostevšek, N.; Gardonio, S.; Fanetti, M.; Valant, M. Inherent Surface Properties of Adsorbent-Free Ultrathin Bi₂Se₃ Topological Insulator Platelets. *Sci. Rep.* **2019**, *9*, 190571. [[CrossRef](#)]
8. Liu, Y.; Zhang, Y.; Zhao, Z.; Jia, G. High Efficient Photothermal Energy Conversion of TI BIS Nanosheets Thin Film. *AIP Adv.* **2018**, *8*, 055013. [[CrossRef](#)]
9. Xie, H.; Li, Z.; Sun, Z.; Shao, J.; Yu, X.F.; Guo, Z.; Wang, J.; Xiao, Q.; Wang, H.; Wang, Q.Q.; et al. Metabolizable Ultrathin Bi₂Se₃ Nanosheets in Imaging-Guided Photothermal Therapy. *Small* **2016**, *12*, 4136–4145. [[CrossRef](#)]
10. Li, Z.; Hu, Y.; Howard, K.A.; Jiang, T.; Fan, X.; Miao, Z.; Sun, Y.; Besenbacher, F.; Yu, M. Multifunctional Bismuth Selenide Nanocomposites for Antitumor Thermo-Chemotherapy and Imaging. *ACS Nano* **2016**, *10*, 984–997. [[CrossRef](#)]
11. Li, Z.; Liu, J.; Hu, Y.; Howard, K.A.; Li, Z.; Fan, X.; Chang, M.; Sun, Y.; Besenbacher, F.; Chen, C.; et al. Multimodal Imaging-Guided Antitumor Photothermal Therapy and Drug Delivery Using Bismuth Selenide Spherical Sponge. *ACS Nano* **2016**, *10*, 9646–9658. [[CrossRef](#)]
12. Li, J.; Jiang, F.; Yang, B.; Song, X.R.; Liu, Y.; Yang, H.H.; Cao, D.R.; Shi, W.R.; Chen, G.N. Topological Insulator Bismuth Selenide as a Theranostic Platform for Simultaneous Cancer Imaging and Therapy. *Sci. Rep.* **2013**, *3*, 1998. [[CrossRef](#)]
13. Zhang, X.-D.; Chen, J.; Min, Y.; Park, G.B.; Shen, X.; Song, S.-S.; Sun, Y.-M.; Wang, H.; Long, W.; Xie, J.; et al. Metabolizable Bi₂Se₃ Nanoplates: Biodistribution, Toxicity, and Uses for Cancer Radiation Therapy and Imaging. *Adv. Funct. Mater.* **2014**, *24*, 1718–1729. [[CrossRef](#)]
14. Batool, Z.; Akhtar, M.; Hasnain, A.U.; Buzdar, S.A.; Ullah, H.; Nazir, A.; Ishtiaq, J.; Rasheed, M. Simple Synthesis of Multifunctional Bismuth Selenide Nanoparticles; Structural, Optical Characterizations and their Effective Antibacterial Activity. *Appl. Phys. A* **2021**, *127*, 833. [[CrossRef](#)]
15. Sobolev, V.V.; Shutov, S.D.; Popov, Y.V.; Sestatskii, S.N. Reflectivity spectra of the rhombohedral crystals Bi₂Te₃, Bi₂Se₃, and Sb₂Te₃ over the range from 0.7 to 12.5 eV. *Phys. Status Solidi* **1968**, *30*, 349–355. [[CrossRef](#)]
16. Zhang, W.; Yu, R.; Zhang, H.-J.; Dai, X.; Fang, Z. First-principles studies of the three-dimensional strong topological insulators Bi₂Te₃, Bi₂Se₃ and Sb₂Te₃. *New J. Phys.* **2010**, *12*, 065013. [[CrossRef](#)]
17. Zhang, H.; Liu, C.-X.; Qi, X.-L.; Dai, X.; Fang, Z.; Zhang, S.-C. Topological insulators in Bi₂Se₃, Bi₂Te₃ and Sb₂Te₃ with a single Dirac cone on the surface. *Nat. Phys.* **2009**, *5*, 438–442. [[CrossRef](#)]
18. Albanese, A.; Tang, P.S.; Chan, W.C. The Effect of Nanoparticle, Size, Shape and Surface Chemistry on Biological Systems. *Annu. Rev. Biomed. Eng.* **2012**, *14*, 1–16. [[CrossRef](#)]

19. Rivera-Gil, P.; Jimenez de Aberasturi, D.; Wulf, V.; Pelaz, B.; del Pino, P.; Zhao, Y.; de la Fuente, J.M.; Ruiz de Larramendi, I.; Rojo, T.; Liang, X.J.; et al. The Challenge to Relate the Physicochemical Properties of Colloidal Nanoparticles to Their Cytotoxicity. *Acc. Chem. Res.* **2013**, *46*, 743–749. [[CrossRef](#)]
20. Nel, A.; Xia, T.; Madler, L.; Li, N. Toxic Potential of Materials at the Nanolevel. *Science* **2006**, *311*, 622–627. [[CrossRef](#)]
21. Nel, A.E.; Mädler, L.; Velegol, D.; Xia, T.; Hoek, E.M.V.; Somasundaran, P.; Klaessig, F.; Castranova, V.; Thompson, M. Understanding Biophysicochemical Interactions at the Nano–bio Interface. *Nat. Mater.* **2009**, *8*, 543–557. [[CrossRef](#)]
22. Verma, A.; Stellacci, F. Effect of Surface Properties on Nanoparticle–Cell Interactions. *Small* **2010**, *6*, 12–21. [[CrossRef](#)]
23. Batabyal, S.K.; Basu, C.; Das, A.R.; Sanyal, G.S. Solvothermal synthesis of bismuth selenide nanotubes. *Mater. Lett.* **2006**, *60*, 2582–2585. [[CrossRef](#)]
24. Wang, D.; Yu, D.; Mo, M.; Liu, X.; Qian, Y. Preparation and characterization of wire-like Sb₂Se₃ and flake-like Bi₂Se₃ nanocrystals. *J. Cryst. Growth* **2003**, *253*, 445–451. [[CrossRef](#)]
25. Wu, X.; Tan, C.; Wang, Q.; Guo, Y.; Wang, D.; Wang, Y.; Meng, D. Solution Growth of Two-Dimensional Bi(2)Se(3) Nanosheets for Two-Color All-Optical Switching. *Materials* **2017**, *10*, 1332. [[CrossRef](#)]
26. Min, Y.; Moon, G.D.; Kim, B.S.; Lim, B.; Kim, J.S.; Kang, C.Y.; Jeong, U. Quick, controlled synthesis of ultrathin Bi₂Se₃ nanodiscs and nanosheets. *J. Am. Chem. Soc.* **2012**, *134*, 2872–2875. [[CrossRef](#)]
27. Li, Z.; Chen, H.; Bao, H.; Gao, M. One-pot reaction to synthesize water-soluble magnetite nanocrystals. *Chem. Mater.* **2004**, *16*, 1391–1393. [[CrossRef](#)]
28. Liu, X.; Xu, J.; Fang, Z.; Lin, L.; Qian, Y.; Wang, Y.; Ye, C.; Ma, C.; Zeng, J. One-pot synthesis of Bi₂Se₃ nanostructures with rationally tunable morphologies. *Nano Res.* **2015**, *8*, 3612–3620. [[CrossRef](#)]
29. Moore, M.M.; Kanekar, S.G.; Dhamija, R. Ethylene Glycol Toxicity: Chemistry, Pathogenesis, and Imaging. *Radiol. Case Rep.* **2008**, *3*, 122. [[CrossRef](#)]
30. Hanafy, B.I.; Cave, G.W.V.; Barnett, Y.; Pierscionek, B. Ethylene Glycol Coated Nanoceria Protects Against Oxidative Stress in Human Lens Epithelium. *RSC Adv.* **2019**, *9*, 16596–16605. [[CrossRef](#)]
31. Hovda, K.E.; Guo, C.; Austin, R.; McMartin, K.E. Renal Toxicity of Ethylene Glycol Results from Internalization of Calcium Oxalate Crystals by Proximal Tubule Cells. *Toxicol. Lett.* **2010**, *192*, 365–372. [[CrossRef](#)]
32. Patlolla, A.K.; Kumari, S.A.; Tchounwou, P.B. A Comparison of Poly-Ethylene-Glycol-Coated and Uncoated Gold Nanoparticle-Mediated Hepatotoxicity and Oxidative Stress in Sprague Dawley Rats. *Int. J. Nanomed.* **2019**, *14*, 639–647. [[CrossRef](#)]
33. FDA. Ethylene Glycol and Propylene Glycol Toxicity. Available online: https://www.atsdr.cdc.gov/csem/ethylene-propylene-glycol/regulations_guidelines.html (accessed on 16 November 2022).
34. Li, Z.; Hu, Y.; Chang, M.; Howard, K.A.; Fan, X.; Sun, Y.; Basenbacher, F.; Yu, M. Highly porous PEGylated Bi₂S₃ nano-urchins as a versatile platform. *nANOSCALE* **2016**, *8*, 35. [[CrossRef](#)]
35. Karimi, Z.; Karimi, L.; Shokrollahi, H. Nano-magnetic particles used in biomedicine: Core and coating materials. *Mater. Sci. Eng. C Mater. Biol. Appl.* **2013**, *33*, 2465–2475. [[CrossRef](#)]
36. Li, R.; He, Y.; Zhang, S.; Qin, J.; Wang, J. Cell membrane-based nanoparticles: A new biomimetic platform for tumor diagnosis and treatment. *Acta Pharm. Sin. B* **2018**, *8*, 14–22. [[CrossRef](#)]
37. Alcantar, N.A.; Aydil, E.S.; Israelachvili, J.N. Polyethylene glycol-coated biocompatible surfaces. *J. Biomed. Mater. Res.* **2000**, *51*, 343–351. [[CrossRef](#)]
38. Diab, R.; Canilho, N.; Pavel, I.A.; Haffner, F.B.; Girardon, M.; Pasc, A. Silica-Based Systems for Oral Delivery of Drugs, Macromolecules and Cells. *Adv. Colloid. Interface Sci.* **2017**, *249*, 346–362. [[CrossRef](#)]
39. FDA. Notification of the GRAS Determination of Silicon Dioxide When Added Directly or Indirectly to Human Food. 2009. Available online: <http://www.fda.gov/Food/FoodIngredientsPackaging/GenerallyRecognizedasSafeGRAS/GRASListings/default.htm> (accessed on 1 December 2022).
40. EFSA; Younes, M.; Aggett, P.; Aguilar, F.; Crebelli, R.; Dusemund, B.; Filipic, M.; Frutos, M.J.; Galtier, P.; Gott, D.; et al. Re-evaluation of silicon dioxide (E 551) as a food additive. *EFSA J. Eur. Food Saf. Auth.* **2018**, *16*, e05088.
41. Zhao, Y.; Sun, X.; Zhang, G.; Rewyn, B.G.T.; Slowing, I.I.; Lin, V.S.-Y. Interaction of Mesoporous Silica Nanoparticles with Human Red Blood Cell Membranes: Size and Surface Effects. *ACS Nano* **2011**, *5*, 1366–1375. [[CrossRef](#)]
42. Chen, L.; Liu, J.; Zhang, Y.; Kang, Y.; Chen, A.; Feng, X.; Shao, L. The toxicity of Silica Nanoparticles to the Immune System. *Nanomedicine* **2018**, *13*, 1939–1962. [[CrossRef](#)]
43. Naprieska, D.; Thomassen, L.C.; Lison, D.; Martens, J.A.; Hoet, P.H. The Nanosilica hazard: Another Variable Entry. *Part. Fibre Toxicol.* **2010**, *7*, 39. [[CrossRef](#)]
44. Hudson, S.P.; Padera, R.F.; Langer, R.; Kohane, D.S. The Biocompatibility of Mesoporous Silicates. *Biomaterials* **2008**, *29*, 4045–4055. [[CrossRef](#)]
45. Santos, H.A. *Porous Silicon for Biomedical Applications*; Wodhead Publishing: Sawston, UK, 2014.
46. Yang, Y.; Zhang, M.; Song, H.; Yu, C. Silica-Based Nanoparticles for Biomedical Applications: From Nanocarriers to Biomodulators. *Acc. Chem. Res.* **2020**, *53*, 1545–1556. [[CrossRef](#)]
47. Huang, R.; Shen, Y.W.; Guan, Y.Y.; Jiang, Y.X.; Wu, Y.; Rahman, K.; Zhang, L.J.; Liu, H.J.; Luan, X. Mesoporous Silica Nanoparticles: Facile Surface Functionalization and Versatile Biomedical Applications in Oncology. *Acta Biomater.* **2020**, *116*, 1–15. [[CrossRef](#)]
48. Wang, Y.; Zhao, Q.; Han, N.; Bai, L.; Li, J.; Liu, J.; Che, E.; Hu, L.; Zhang, Q.; Jiang, T.; et al. Mesoporous Silica Nanoparticles in Drug Delivery and Biomedical Applications. *Nanomedicine* **2015**, *11*, 313–327. [[CrossRef](#)]

49. Liu, S.; Han, M.-Y. Silica-Coated Metal Nanoparticles. *Chem. Asian J.* **2009**, *5*, 36–45. [[CrossRef](#)]
50. Guerrero-Martínez, A.; Pérez-Juste, J.; Liz-Marzán, L.M. Recent Progress on Silica Coating of Nanoparticles and Related Nanomaterials. *Adv. Mater.* **2010**, *22*, 1182–1195. [[CrossRef](#)]
51. Goršak, T.; Makovec, D.; Javornik, U.; Belec, B.; Kralj, S.; Lisjak, D. A Functionalization Strategy for the Dispersion of Permanently Magnetic Barium-Hexaferrite Nanoplatelets in Complex Biological Media. *Colloids Surf. A Physicochem. Eng. Asp.* **2019**, *573*, 119–127. [[CrossRef](#)]
52. Kralj, S.; Potrč, T.; Kocbek, P.; Marchesan, S.; Makovec, D. Design and Fabrication of Magnetically Responsive Nanocarriers for Drug Delivery. *Current. Med. Chem.* **2017**, *24*, 454–469. [[CrossRef](#)]
53. Rožič, B.; Jagodič, M.; Gyergyek, S.; Drogenik, M.; Kralj, S.; Jagličič, Z.; Kutnjak, Z. Mixtures of magnetic nanoparticles and the ferroelectric liquid crystal: New soft magnetoelectrics. *Ferroelectrics* **2012**, *21*, 150–153. [[CrossRef](#)]
54. Kralj, S.; Makovec, D.; Čampelj, S.; Drogenik, M. Producing ultra-thin silica coatings on iron-oxide nanoparticles to improve their surface reactivity. *J. Magn. Magn. Mater.* **2010**, *322*, 1847–1853. [[CrossRef](#)]
55. Nemeč, S.; Kralj, S. A Versatile Interfacial Coassembly Method for Fabrication of Tunable Silica Shells with Radially Aligned Dual Mesopores on Diverse Magnetic Core Nanoparticles. *ACS Appl. Mater. Interfaces* **2021**, *13*, 1883–1894. [[CrossRef](#)]
56. Nemeč, S.; Kralj, S.; Wilhelm, C.; Abou-Hassan, A.; Rols, M.-P.; Kolosnjaj-Tabi, J. Comparison of Iron Oxide Nanoparticles in Photothermal and Magnetic Hyperthermia: Effects of Clustering and Silica Encapsulation on Nanoparticles' Heating Yield. *Appl. Sci.* **2020**, *10*, 7322. [[CrossRef](#)]
57. Tadić, M.; Kralj, S.; Lalatonne, Y.; Motte, L. Iron Oxide Nanochains Coated with Silica: Synthesis, Surface Effects and Magnetic Properties. *Appl. Surf. Sci.* **2019**, *476*, 641–646. [[CrossRef](#)]
58. Hu, J.; Gorsak, T.; Martín Rodríguez, E.; Calle, D.; Muñoz-Ortiz, T.; Jaque, D.; Fernández, N.; Cussó, L.; Rivero, F.; Aguilar Torres, R.; et al. Magnetic Nanoplatelets for High Contrast Cardiovascular Imaging by Magnetically Modulated Optical Coherence Tomography. *ChemPhotoChem* **2019**, *3*, 529–539. [[CrossRef](#)]
59. Gorsak, T.; Drab, M.; Krizaj, D.; Jeran, M.; Genova, J.; Kralj, S.; Lisjak, D.; Kralj-Iglic, V.; Iglic, A.; Makovec, D. Magneto-Mechanical Actuation of Barium-Hexaferrite Nanoplatelets for the Disruption of Phospholipid Membranes. *J. Colloid Interface Sci.* **2020**, *579*, 508–519. [[CrossRef](#)]
60. Pham, X.H.; Park, S.M.; Ham, K.M.; Kyeong, S.; Son, B.S.; Kim, J.; Hahm, E.; Kim, Y.H.; Bock, S.; Kim, W.; et al. Synthesis and Application of Silica-Coated Quantum Dots in Biomedicine. *Int. J. Mol. Sci.* **2021**, *22*, 10166. [[CrossRef](#)]
61. Eradhodiyil, N.; Ying, J.Y. Functionalization of Inorganic Nanoparticles for Bioimaging Applications. *Acc. Chem. Res.* **2011**, *44*, 925–935. [[CrossRef](#)]
62. Wu, S.; Li, A.; Zhao, X.; Zhang, C.; Yu, B.; Zhao, N.; Xu, F.J. Silica-Coated Gold-Silver Nanocages as Photothermal Antibacterial Agents for Combined Anti-Infective Therapy. *ACS Appl. Mater. Interfaces* **2019**, *11*, 17177–17183. [[CrossRef](#)]
63. Ferfolja, K.; Valant, M.; Mikulska, I.; Gardonio, S.; Fanetti, M. Chemical Instability of an Interface between Silver and Bi₂Se₃ Topological Insulator at Room Temperature. *J. Phys. Chem. C* **2018**, *122*, 9980–9984. [[CrossRef](#)]
64. Kralj, S.; Makovec, D. Magnetic Assembly of Superparamagnetic Iron Oxide Nanoparticle Clusters into Nanochains and Nanobundles. *ACS Nano* **2015**, *9*, 9700–9707. [[CrossRef](#)]
65. Kashchiev, D. *Nucleation: Basic Theory with Applications*; Butterworth-Heinemann, Elsevier Science: Burlington, NJ, USA, 2000.
66. Zhao, Y.; Dunn, A.; Lin, J.; Shi, D. Photothermal Effect of Nanomaterials for Efficient Energy Applications. In *Micro and Nano Technologies*; Elsevier: Amsterdam, The Netherlands, 2015; pp. 415–434. [[CrossRef](#)]
67. Zhang, H.; Chen, H.-J.; Du, X.; Wen, D. Photothermal Conversion Characteristics of Gold Nanoparticle Dispersions. *Sol. Energy* **2014**, *100*, 141–147. [[CrossRef](#)]
68. Kim, M.; Kim, G.; Kim, D.; Yoo, J.; Kim, D.K.; Kim, H. Numerical Study on Effective Conditions for the Induction of Apoptotic Temperatures for Various Tumor Aspect Ratios Using a Single Continuous-Wave Laser in Photothermal Therapy Using Gold Nanorods. *Cancers* **2019**, *11*, 764. [[CrossRef](#)]
69. Zhang, Y.; Zhan, X.; Xiong, J.; Peng, S.; Huang, W.; Joshi, R.; Cai, Y.; Liu, Y.; Li, R.; Yuan, K.; et al. Temperature-dependent cell death patterns induced by functionalized gold nanoparticle photothermal therapy in melanoma cells. *Sci. Rep.* **2018**, *8*, 8720. [[CrossRef](#)]
70. Roti Roti, J.L. Cellular responses to hyperthermia (40–46 degrees C): Cell killing and molecular events. *Int. J. Hyperth.* **2008**, *24*, 3–15. [[CrossRef](#)]
71. Leber, B.; Mayrhauser, U.; Leopold, B.; Koestenbauer, S.; Tscheliessnigg, K.; Stadlbauer, V.; Steigled, P. Impact of Temperature on Cell Death in a Cell-culture Model of Hepatocellular Carcinoma. *Anticancer Res.* **2012**, *32*, 915–922.
72. Khashan, S.; Dagher, S.; Al Omari, S.; Tit, N.; Elnajjar, E.; Mathew, B.; Hilal-Alnaqbi, A. Photo-thermal characteristics of water-based Fe₃O₄@SiO₂ nanofluid for solar-thermal applications. *Mater. Res. Express* **2017**, *4*, 055701. [[CrossRef](#)]
73. Mallah, A.R.; Zubir, M.N.M.; Alawi, O.A.; Kazi, M.S.N.; Ahmed, S.M.; Oon, C.S.; Mohamad, A.B. An innovative, high-efficiency silver/silica nanocomposites for direct absorption concentrating solar thermal power. *Int. J. Energy Res.* **2020**, *44*, 9438–9453. [[CrossRef](#)]

Disclaimer/Publisher's Note: The statements, opinions and data contained in all publications are solely those of the individual author(s) and contributor(s) and not of MDPI and/or the editor(s). MDPI and/or the editor(s) disclaim responsibility for any injury to people or property resulting from any ideas, methods, instructions or products referred to in the content.